A Second Generation Swirl-Venturi Lean Direct Injection Combustion Concept

Kathleen M. Tacina*, Clarence T. Chang* and Zhuohui Joe He*
NASA Glenn Research Center, Cleveland, Ohio, 44135

Phil Lee† and Bidhan Dam‡
Woodard FST, Zeeland, Michigan, 49464

Hukam Mongia §
Purdue University, West Lafayette, Indiana, 47907

A low-NO_x aircraft gas turbine engine combustion concept was developed and tested. The concept is a second generation swirl-venturi lean direct injection (SV-LDI) concept. LDI is a lean-burn combustion concept in which the fuel is injected directly into the flame zone. Three second generation SV-LDI configurations were developed. All three were based on the baseline 9-point SV-LDI configuration reported previously.[1] These second generation configurations had better low power operability than the baseline 9-point configuration. Two of these second generation configurations were tested in a NASA Glenn Research Center flametube; these two configurations are called the flat dome and 5-recess configurations. Results show that the 5-recess configuration generally had lower NO_x emissions than the flat dome configuration. Correlation equations were developed for the flat dome configuration so that the landing-takeoff NO_x emissions could be estimated. The flat dome landing-takeoff NO_x is estimated to be 87–88% below the CAEP/6 standards, exceeding the ERA project goal of 75% reduction.

I. Introduction

For more than 40 years, NASA has sustained programs to reduce the environmental effects of aviation. A major focus of these programs has been reducing the emissions of nitrogen oxides (NO_x) while simultaneously reducing emissions of carbon monoxide (CO), unburned hydrocarbons, and smoke and meeting other combusition design requirements including operability and durability. NO_x emissions increase smog and ozone in the lower troposphere and decrease the protective ozone layer in the stratosphere.[2]

Currently, the Environmentally Responsible Aviation (ERA) project aims to reduce the engine specific fuel consumption by 15% and the emissions of NO_x by 75%; these goals apply to N+2 concepts that will enter service by 2025. In order to reduce specific fuel consumption, engines will need to increase the operating pressure ratio, thus increasing the combustor inlet pressure and temperature. However, NO_x formation rates increase with higher temperatures. To decrease NO_x by 75% while simultaneously reducing specific fuel consumption, improved low-NO_x combustor technologies need to be developed. Under an ERA project contract with NASA, Woodward FST, has developed a low-NO_x N+2 combustor concept.

In order to reduce NO_x emissions, NASA has investigated several combustion concepts. These concepts fall into two categories: rich-front-end and lean-front-end. Rich-front-end combustors are similar to traditional combustors in that the primary combustion zone is fuel-rich—only part of the combustion air

*Aerospace Engineer, Combustion Branch
†Engineer, AIAA member
‡Engineer
§Visiting Professor, School of Mechanical Engineering, AIAA Fellow

enters through the fuel/air mixers; the rest enters downstream through a set of primany and dilution jets to complete combustion to be completed and meet exit temperature quality requirements including profile and pattern factor. All modern rich-front-end combustors entering revenue serivec since 1995 use rich-burn-quick quench-lean-burn (RQL) combustion techniques to simultaneously minimize NO_x and smoke emissions.[3–5] In contrast, lean-front-end combustors operate fuel-lean throughout: All of the combustor air except that used for liner cooling enters through the combustor dome. Lean -front-end combustion concepts include lean, premixed, prevaporized (LPP), lean partially premixed, and lean direct injection (LDI) combustion.[1,3,6–10] This paper focuses on a LDI combustion concept.

As the name implies, in LDI the combustor operates fuel-lean without a rich front end. All of the combustor air except that used for liner cooling enters through the combustor dome. Like other lean burn combustion concepts, LDI reduces NO_x emissions by minimizing flame temperature, since NO_x is an exponential function of temperature. To eliminate local hot spots that produce high levels of NO_x, lean burn combustion concepts rely on the fuel and air being well-mixed before burning occurs. Thus, LDI requires rapid fuel vaporization and uniform fuel-air mixing. LDI achieves this by using a multi- element concept with small fuel/air mixers.

Several fuel-air mixing strategies have been studied for LDI fuel/air mixers. There are several ways an individual fuel/air mixer (the fuel injector) can be constructed. On the air side, a radial,[8] axial,[1,7] or discrete jet swirler[9] may be used. A venturi can be placed downstream of the air swirler, or the venturi can be omitted. On the fuel side, a simplex or air assist atomizer can be used. For a simplex atomizer, flow number (i.e., effective flow area) can be varied. In addition, once a fuel/air mixer design has been chosen, the size and number of the mixer elements can be varied.

The LDI design that has been studied most extensively is the 9-point swirl-venturi LDI (SV-LDI) design.[1,7,10] This baseline design consists of 9 identical fuel/air mixers arranged in a 3x3 grid with a 76.2-mm by 76.2-mm square cross section. Each fuel/air mixer consists of a simplex fuel injector and an air passage with an axial air swirler followed by a converging-diverging venturi section. The baseline 9-point SV-LDI design was initially developed under the High Speed Research (HSR) program in the 1990s, and it showed a substantial reduction in NO_x emissions compared to the then-current state-of-the-art. However, the NO_x emissions were not low enough to meet the most stringent ERA requirement of 75% NO_x reduction. In addition, the baseline 9-point SV-LDI did not perform well at low power conditions. Good operation at low power conditions is required for ERA combustor concepts.

Therefore, to meet the ERA goals of 75% NO_x reduction and good low power operation, Woodward developed a second-generation SV-LDI concept. Although this design is based upon the baseline 9-point concept, it includes advanced features designed to reduce NO_x emissions and improve low power operation; these advanced features included airblast tips and a pilot fuel/air mixer,

Three distinct second-generation SV-LDI configurations were developed. Two of these configurations were tested at flametube facilities at Woodward FST, and NASA Glenn Research Center; these two configurations are described in section IIC below. Testing was done at inlet pressures up to 1790 kPa and inlet temperatures up to 855 K.

This paper presents emissions results from the NASA Glenn flametube testing of this second-generation LDI design. Emissions results from each configuration are shown and compared to each other and to emissions correlations based on the baseline 9-point SV-LDI design.

II. Experimental Facilities and Hardware

A. Experimental Facilities and Data Analysis

These tests were done in NASA Glenn's flametube combustion test rigs. A sketch of a flametube is shown in Fig. 1. This facility can supply nonvitiated air preheated to 865 K at pressures up to 3.1 MPa. The flametube can be configured to use different test sections with varying cross-sectional area. For the baseline 9-point SV-LDI experiments previously described in R. Tacina et al,[1] the flametube test section was configured to have a 76.2-mm × 76.2-mm square cross section that could handle pressures up to 3.1 MPa. For the second-generation LDI experiments described in this paper, the flametube test section was configured to have a 114.3-mm × 114.3-mm square cross section that could handle pressures up to 1.9 MPa at an inlet air temperature of 825 K or 1.7 MPa at an inlet air temperature of 865 K. Both flametubes had ceramic liners downstream of the dump plane. A 5-hole probe is used to measure gaseous emissions.

The test rig supports up to three fuel circuits. The fuel used in typically JP-8. However, an alternative

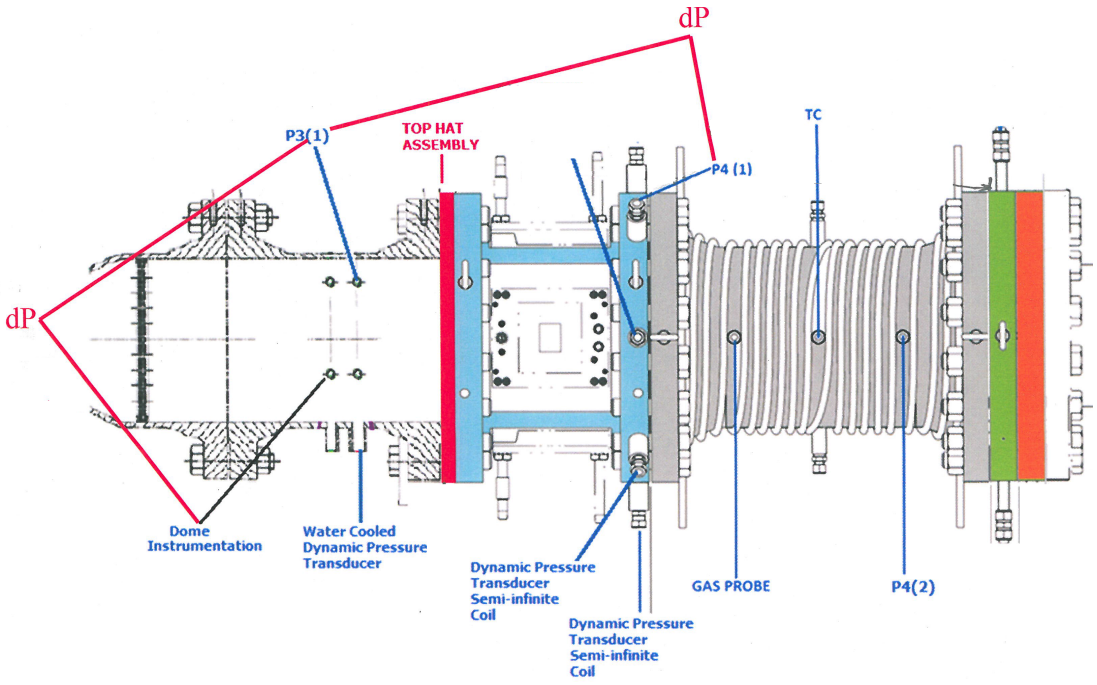

Figure 1: *The flametube used for testing the second generation SV-LDI configurations.*

Table 1: *Combustion conditions: inlet temperature, T_3, and pressure, p_3*

p_3 (across) T_3 (down)	0.7 MPa (100 psia)	1.0 MPa (150 psia)	1.4 MPa (200 psia)	1.7 MPa (250 psia)	1.6 MPa (230 psia)	1.8 MPa (260 psia)
535 K (500 F)	x	x	x			
650 K (700 F)	x		x	x		
755 K (900 F)		x	x	x		
825 K (1020 F)		x	x	x		
860 K (1090 F)		x	x		x	
810 K (1000 F)						x

jet fuel (e.g., a biofuel) can also be used. JP-8 and the biofuel can be mixed on-the-fly during testing.

The test rig is equipped with a standard gas bench to measure CO_2, CO, O_2, NO_x, and unburned hydrocarbons so that emissions can be measured according to the SAE Aerospace Recommend Practice (ARP) 1256.[11] More details on NASA Glenn's flametube combustion test rigs can be found in Bianco.[12]

Emissions measurements are analyzed according to SAE ARP 1533.[13] Adiabatic flame temperatures are calculated using the Chemical Equilibrium for Applications (CEA) equilibrium code.[14]

B. Testing Strategy

Testing parameters were varied as systematically as was possible with the limited testing time and facility capabilities. Most testing was done at four inlet temperatures: 535 K (500 F), 650 K (700 F), 755 K (900 F), and the maximum normal operating temperature 825 K (1020 F). At each of these inlet temperatures, we went tested at three inlet pressures. At lower inlet temperatures, corresponding to lower inlet pressures, the lowest inlet pressure was 0.7 MPa (100 psia); at higher inlet temperatures, it was 1.0 MPa (150 psia). Some data was also taken at the maximum operating pressure of 1.8 MPa (260 psia) at a temperature slightly below the maximum (1000 F instead of 1020 F). In addition, during the flat dome testing we were able to increase the maximum operating temperature to 860 K (1090 F) at the cost of reducing the maximum

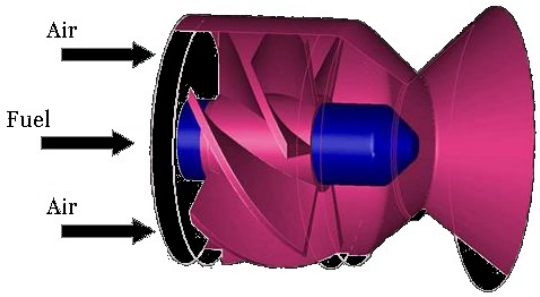

Figure 2: *A single SV-LDI fuel/air mixer.*

Figure 3: *Baseline 9-point SV-LDI design. From R. Tacina et al.*[1]

pressure to 1.6 MPa (230 psia). A grid of the test conditions is shown in Table 1.

During the flat dome test, we had enough testing time to vary the dome pressure drop $\Delta p/\mathrm{p}$; we used 3%, 4%, and 5%. However, there was no time to vary the pressure drop in 5-recess test; during this test, we tested with alternative fuel in addition to JP-8, but the testing time was not increased. As a result, the dome pressure drop was kept fixed at 3%.

C. LDI Hardware

The current second-generation SV-LDI configurations were based upon the initial baseline 9-point SV-LDI concept developed under NASA's HSR and UEET programs. Therefore, the baseline concept will be described before the current second-generation SV-LDI hardware is described.

As shown in Fig. 2, a SV-LDI fuel/air mixer consists of a fuel injector and an air passage with an axial air swirler followed by a converging-diverging venturi section. The fuel injector is inserted through the center of the air swirler, with the tip typically located at the venturi throat.

As shown in Fig. 3, the baseline 9-point configuration consists of 9 SV-LDI fuel/air mixers arranged in a 3 × 3 grid with a 76.2-mm × 76.2-mm square cross-section. The center-to-center distance between fuel/air mixers is 25.4 mm. The air swirlers each have 6 helical blades, with a blade angle of 45°, 52.5°, or 60°; the blades can have either a clockwise or counterclockwise orientation. The fuel injector is a simplex injector and the injector tip sits at the venturi throat. Except for possible differences in air swirler angle and orientation, each fuel/air mixer is identical. The measured effective area of the 9-point configuration is 955 mm^2 for 45° swirlers, 925 mm^2 for the 52.5° swirlers, and 870 mm^2 for the 60° swirlers.

Results from the baseline configuration guided the design of the second-generation SV-LDI hardware. One major concern was operability. Although baseline results showed that reducing the swirler angle typically reduced $\mathrm{NO_x}$ emissions, reducing the swirler angle also reduced operability.[1] The baseline configuration with the 45° swirlers would have met the ERA $\mathrm{NO_x}$ emissions goals, but the operability would have been unacceptable. In addition, limited experiments showed that fuel staging did not significantly extend low-power operability; this lack of success in fuel staging was attributed to mixing between adjacent fuel-air mixers.[1]

Like the baseline configuration, the second-generation SV-LDI configurations consists of multiple SV-LDI fuel/air mixers: 13 fuel/air mixers arranged in a 114.3 mm × 114.3 mm square cross-section. However, unlike in the baseline configuration, the fuel/air mixers are not identical. First, to address operability concerns, a

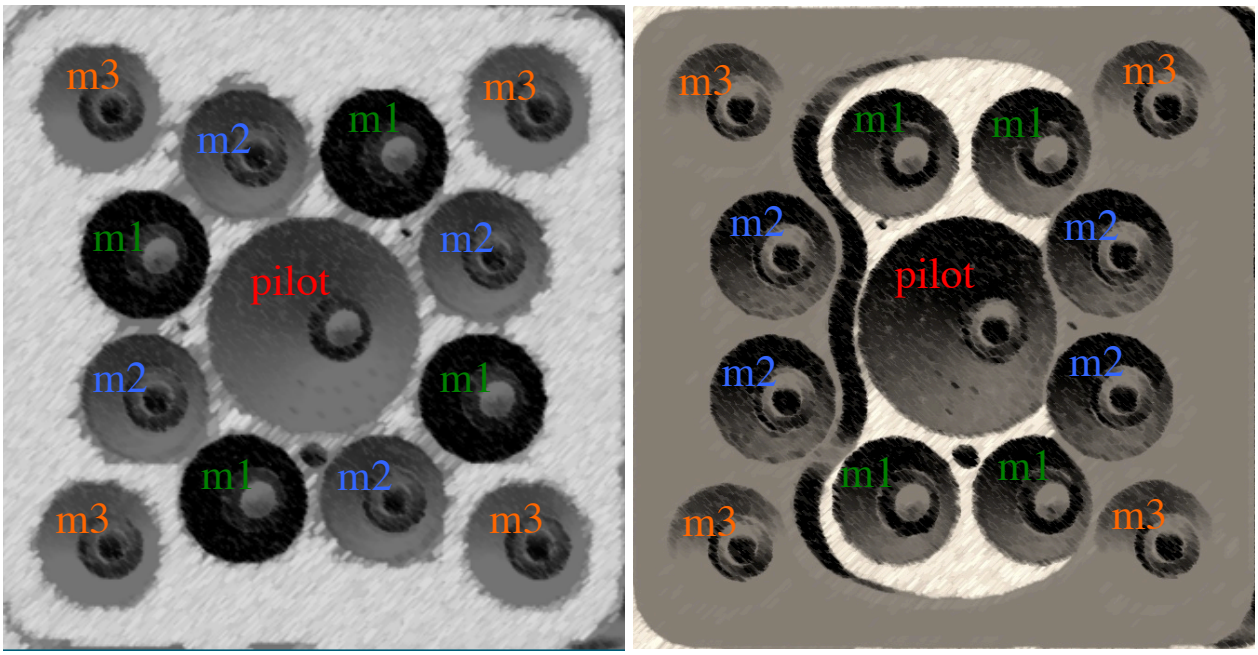

(a) *(b)*

Figure 4: *Second generation SV-LDI hardware: (a) flat dome and (b) 5-recess configurations.*

pilot stage was added. The pilot stage was a single fuel/air mixer that was slightly larger than the fuel/air mixers used in the main stage. It was larger in part because the diverging section of the venturi was extended; this venturi extension limited mixing with the adjacent main stages. In addition to adding the pilot stage, the main stage was subdivided into into three parts, called main 1, main 2, and main 3. Each of these main stages consisted of four fuel/air mixers, for a total of 12 main fuel/air mixers. These twelve fuel/air mixers had the same venturi geometry (e.g., the venturi throat and exit diameters were the same for all 12 main fuel/air mixers). In addition, for a given stage, each fuel/air mixer was identical. However, the fuel/air mixers were configured differently for each stage: both the fuel injector type (simplex or airblast) and the air swirler angle(s) differed.

Two second-generation SV-LDI configurations were tested: these configurations are called the flat dome configuration and the 5-recess configuration. Both are shown in Fig. 4 and some important parameters are given in Table 2. The configurations are similar in many respects. For both, the main 1 fuel injectors are simplex and the main 2 and 3 fuel injectors are airblast. In addition, the swirler angles for the main stages are the same, although the orientations are different. The effective areas are also similar, 1284 mm^2 for the

Table 2: *Second Generation SV-LDI configurations. For each stage, the table gives the type of fuel injector and the air swirler angle(s). (OAS: outer air swirler, IAS: inner air swirler, cw=clockwise, ccw=counterclockwise)*

Configuration	Pilot Injector	Pilot Swirler	Main 1 Injector	Main 1 Swirler	Main 2 Injector	Main 2 Swirler	Main 3 Injector	Main 3 Swirler
Flat Dome	Simplex	55°ccw	Simplex	45°ccw	Airblast	IAS: 45°cw OAS: 45°cw	Airblast	IAS: 45°cw OAS: 45°cw
5-Recess	Airblast	IAS: 57°cw OAS: 57°ccw	Simplex	45°cw	Airblast	IAS: 45°cw OAS: 45°ccw	Airblast	IAS: 45°cw OAS: 45°ccw

flat dome configuration and 1318 mm^2 for the 5-recess configuration. However, the configurations differ in two respects. First, the pilot fuel injector is a simplex for the flat dome configuration and an airblast for the 5-recess configuration. Second, the dome geometry is different: in the 5-recess configuration, the pilot and main 1 stages are recessed from the dump plane.

Note that each configuration has 4 stages, a pilot stage and three main stages. However, the test cell only supports three fuel circuits. Therefore, the fuel lines for two stages needed to be ganged together. For the flat dome configuration, the main 2 and main 3 fuel lines were ganged together. For the 5-recess configuration, the pilot and main 2 fuel lines were ganged together; this resulted in the pilot stage being slightly richer than the main 2 stage.

III. Results

Lean blowout tests conducted at Woodward showed that the second generation SV-LDI designs had improved low power operability, with a lean blowout occurring at fuel-air ratios below 0.006.

The rest of this paper concentrates on NO_x emissions at higher power. First, we compare the NO_x emissions from the two second generation SV-LDI configurations to each other. Then, we consider the effect of combustor inlet conditions for both second generation configurations and of dome pressure drop for the flat dome configuration. After that, we compare the NO_x emissions when an alternative fuel is burned to the NO_x emissions when burning JP-8; this is done for the 5-recess configuration. Finally, we develop correlation equations for the flat dome configuration, calculate the landing-takeoff NO_x emissions for this configuration, and compare the flat dome NO_x emissions to NO_x emissions predicted by the first-generation SV-LDI correlation equations.

Although fuel staging was investigated, this paper only presents results where each stage had the same fuel-air ratio. This excludes all data at idle and near-idle conditions (e.g., 535 K = 500 F); during these low power conditions, some of the stages were turned off. It also excludes higher power points where all stages were on but the stages did not have equal fuel-air ratios; for example, cases where the pilot stages was made leaner than the other stages to see if this would reduce the NO_x. (It turned out that making the pilot more fuel-lean did not help: the NO_x emissions were generally lowest when all stages had the same fuel-air ratio.)

Most of the results are presented as plots of the NO_x emissions index vs. adiabatic flame temperature, T_{ad}. Presenting the results instead as plots of NO_x emissions index vs. the equivalence ratio ϕ would not affect the conclusions. This can be seen by comparing Fig. 5 and 6. These figures plot NO_x emissions at a constant inlet pressure as functions of adiabatic flame temperature and equivalence ratio, respectively. Comparing these two figures show that similar conclusions can be reached by examining either figure: the shape of the NO_x vs. ϕ curves are qualitatively similar to the shapes of the NO_x vs. T_{ad} curves. As neither the adiabatic flame temperature nor the equivalence ratio collapse the data, there is no advantage to plotting the NO_x emissions as a function of equivalence ratio. Moreover, plotting the NO_x emissions as a function of flame temperature will minimize the effect that small deviations in inlet temperature have on the plots. Therefore, in subsequent plots the NO_x emissions are plotted against the adiabatic flame temperature.

A. Comparison of Second-Generation SV-LDI Configurations

Figures 6 and 7 compare NO_x emissions from the flat dome configuration to those of the 5-recess configuration. The pressure drop $\Delta p/p$ is 3.%. Figure 6 shows results at a constant inlet pressure and Fig. 7 shows results at a constant inlet temperature. In all three figures, flat dome results are plotted with open symbols and dashed lines and 5-recess results are plotted with closed symbols and solid lines.

The results show that the NO_x emissions from the flat dome configuration are typically either the same or higher than those from the 5-recess configuration. However, whether the emissions are the same or higher does not appear to be a simple trend of inlet temperature, inlet pressure, equivalence ratio, or adiabatic flame temperature.

When the NO_x vs. T_{ad} (or ϕ) curves for the 5-recess configuration are compared with the corresponding curve for the flat dome configuration, four general trends emerge. First, the NO_x emissions from both configurations are nearly the same at all flame temperatures (or equivalence ratios). This occurs at three combustor inlet temperature, pressure pairs: (650 K, 0.7 MPa), (755 K, 1.4 MPa), and (825 K, 1.4 MPa). Second, the NO_x emissions are higher for the flat dome configuration but the slopes of the $\log NO_x$ vs. T_{ad} curves are similar for both configurations. This occurs at two inlet conditions: (650 K, 1.4 MPa) and (650

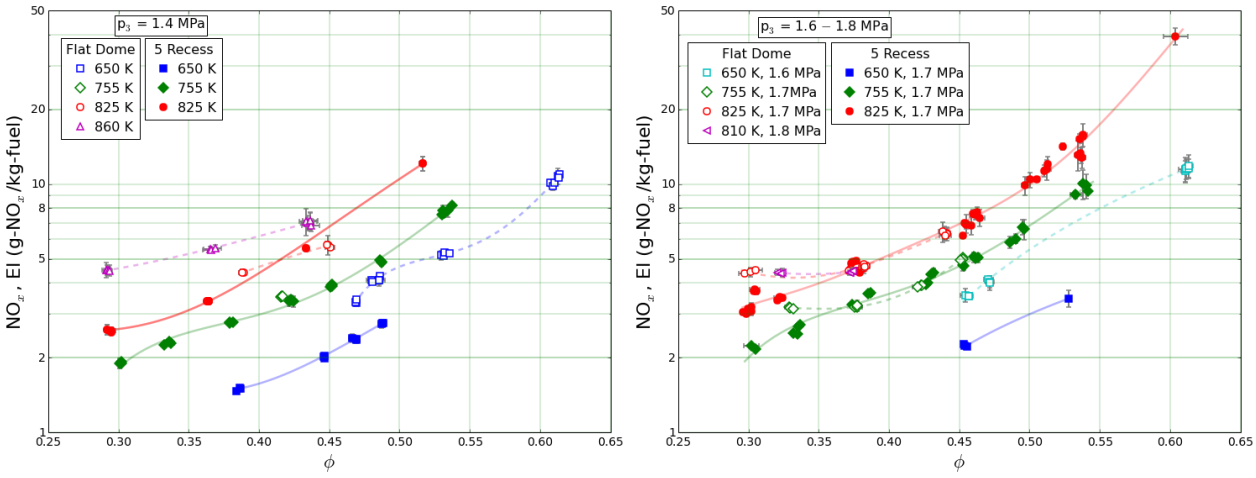

(a) p_3=1.4 MPa *(b) p_3=1.6–1.8 MPa*

Figure 5: *NO_x emissions as a function of equivalence ratio ϕ at constant combustor inlet pressure p_3: (a) 1.4 MPa and (b) 1.6 –1.8 MPa. The pressure drop $\Delta p/p$ is 3%.*

K, 1.7 MPa). Third, the flat dome configuration has higher NO_x emissions at lower flame temperatures but the slope for the flat dome configuration is also flatter; then, when the $\log NO_x$ vs. T_{ad} curves for both configurations intersect, the curves converge so that the NO_x emissions at flame temperatures higher than the intersection point are similar for both configurations. This occurs at inlet conditions of (725 K, 1.7 MPa) and (825 K, 1.7 MPa). It may also occur at two more inlet conditions: (755 K, 1.0 MPa) and (825 K, 1.0 MPa). However, for these latter two conditions, a fourth trend may be happening instead: the flat dome $\log NO_x$ vs. T_{ad} curve is nearly flat even at high flame temperatures, which results in the flat dome configuration having lower NO_x emissions than the 5-recess configurations at high flame temperatures. Distinguishing between these two possibilities requires additional measurements at higher flame temperatures for the flat dome configuration.

B. Effect of Inlet Temperature and Pressure

Figures 6–8 show the effect of inlet temperature and pressure on NO_x emissions. In Fig. 6–7, results are shown from both the 5-recess and flat dome configurations at a pressure drop $\Delta p/p$ of 3%; the 5-recess results are shown by closed symbols and solid lines and the flat dome results by open symbols and dashed lines. In Fig. 8, only flat dome results are shown. However, the results are shown at three pressure drops, 3%, 4%, and 5%; results for 3% pressure drop are shown by closed symbols and solid lines; results for 4% pressure drop by open symbols and dashed lines; and results for 5% pressure drop by yellow-filled symbols and dotted lines.

Figures 5 and 6 show that NO_x emissions consistently increase as combustor inlet temperature increases.

Figures 7 and 8 show that NO_x emissions generally increase as pressure increases. One exception to this trend occurs at an inlet temperature of 650 K for the 5-recess configuration; here, as shown in Fig. 7a, NO_x emissions do not depend on inlet pressure.

A second exception occurs for the flat dome configuration at inlet temperature of 755 K and inlet pressure of 1.0 MPa and a pressure drop of 3%. Figure 7b and 8b show NO_x vs. T_{ad} curves at 755 K. As shown in these figures, at a flame temperature of 1500 K, the NO_x emissions are the same regardless of whether the pressure is 1.0 or 1.7 MPa. Near 1600 K, the NO_x emissions are higher for 1.0 MPa. By 1780 K, the NO_x emissions are lower for 1.0 MPa.

In fact, Fig. 7b and 8b show the the $\log NO_x$ vs. T_{ad} curve has an unexpected shape at inlet conditions of 755 K and 1.0 MPa. This is true for pressure drops of both 3% and 4%. Both the 3% and 4% $\Delta p/p$ are relatively flat; the NO_x emissions index changes by less than 1.0 between flame temperatures of 1500 and 1700 K. In addition, for both curves, there are conditions when an increase in flame temperature leads to a slight decrease in NO_x emissions. This is unexpected but does seem to be repeatable: after finishing the ϕ

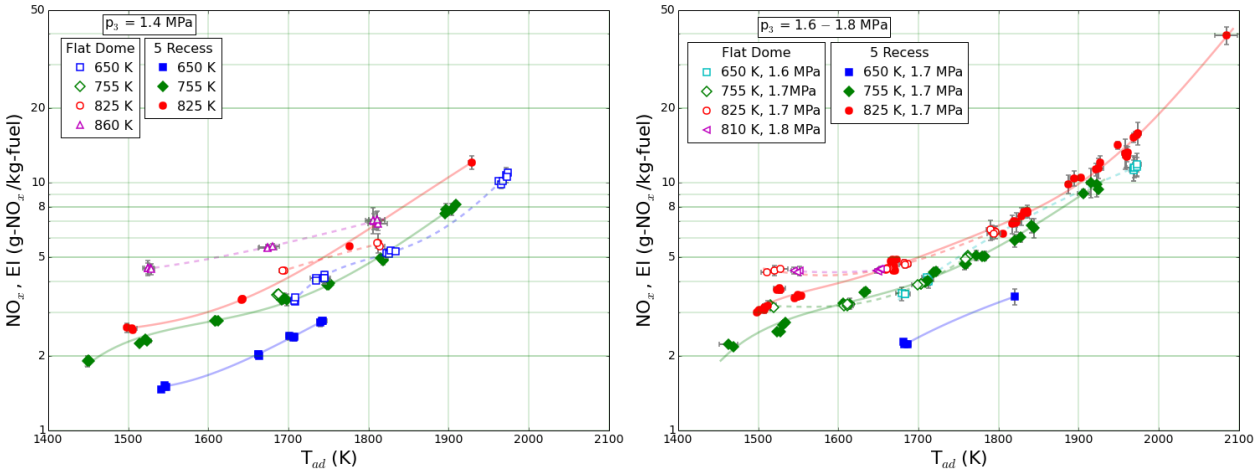

(a) p_3=1.4 MPa *(b) p_3=1.6–1.8 MPa*

Figure 6: *NO_x emissions as a function of equilibrium flame temperature T_{ad} at constant combustor inlet pressure p_3: (a) 1.4 MPa and (b) 1.6 –1.8 MPa. The pressure drop $\Delta p/p$ is 3%.*

sweep at 3% Δp/p, we went back and repeated a few points—the NO_x emissions did not change.

A relatively flat slope of the log NO_x vs. T_{ad} curve may indicate that burning occurs before the fuel is fully vaporized and well-mixed with the combustion air. This should be investigate using optical diagnostics and/or CFD calculations.

C. Effect of Dome Pressure Drop

Figure 8 shows the effect of dome pressure drop on NO_x emissions for the flat dome configuration. Results for 3% pressure drop are shown by closed symbols and solid lines; results for 4% pressure drop by open symbols and dashed lines; and results for 5% pressure drop by yellow-filled symbols and dotted lines.

The results show that increasing the pressure drop generally decreases NO_x emissions. This is expected because the increased pressure drop Δp/p is caused by an increase in the cold flow bulk velocity; this in turn decreases the residence time.

There are some exceptions to this trend. At 650 K and 1.4 MPa, NO_x emissions are similar for pressure drops of 3% and 4%. In addition, there are exceptions at 1.0 MPa for inlet temperatures of 755 K and 860 K. Also note that, even for the majority of cases where NO_x emissions decrease with increasing pressure drop, the amount of the NO_x decrease is not consistent. Both the exceptions to the trend and the inconsistent decreases NO_x emissions could also be caused by the change in the cold flow bulk velocity. A change in cold flow velocity will cause a change in the fuel atomization; this change in fuel atomization will cause a change in fuel vaporization and mixing. Again, optical diagnostic measurements and CFD simulations could help to explain the results.

D. Effect of Alternative Fuel

For the 5-recess configuration, an alternative fuel was used in addition to JP-8 to study the effect of alternative fuel on NO_x emissions. The alternative fuel chosen was made from the Camelina sativa plant. This fuel has properties very similar to JP-8. Table 3 and Fig. 9 compare the properties of the Camelina biofuel to samples of JP-8 taken during (4/25/13) and just after (4/29/13) the testing of the 5-recess configuration. The differences between JP-8 and Camelina are small; the most important difference is that Camelina has a slightly higher H/C ratio, 2.0 vs. 1.9 for JP-8.

This small difference in fuel properties is reflected in the NO_x emissions results. Figure 10 shows NO_x emissions as a function of flame temperature for three different combustor inlet conditions. At each inlet condition, results are shown for at least three mass-based alternative fuel percentages, ranging from 0% alternative fuel (i.e., 100% JP-8) to 100% alternative fuel. For all three inlet conditions, NO_x emissions are

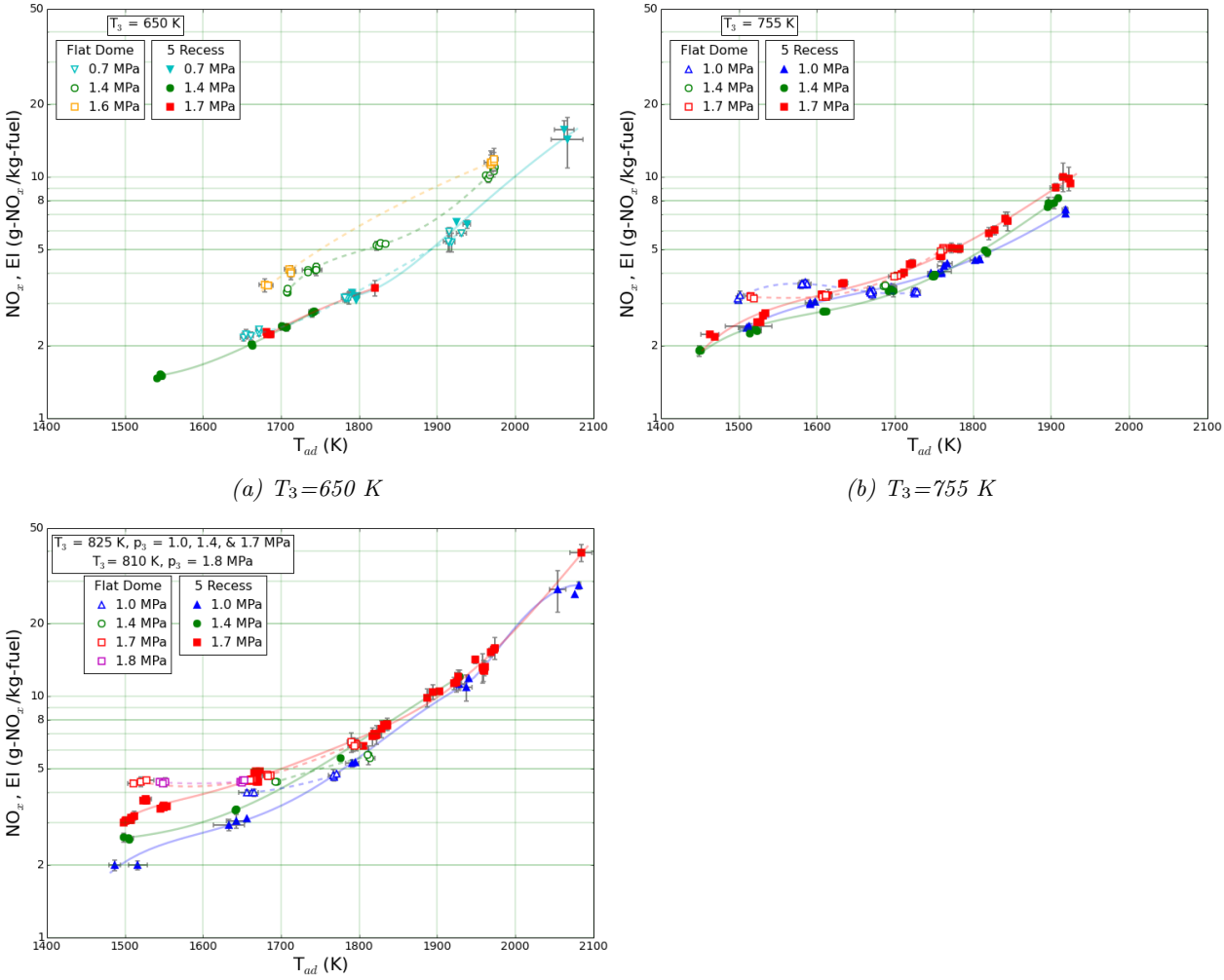

(a) T_3=650 K

(b) T_3=755 K

(c) T_3=810–825K

Figure 7: *NO_x emissions as a function of equilibrium flame temperature T_ad at constant T_3: (a) 650 K, (b) 755 K, and (c) 810–825 K. The pressure drop $\Delta p/p$ is 3%.*

Table 3: *Comparison of JP-8 and alternative fuels.*

Fuel	Carbon % mass	Hydrogen % mass	Sulfur ppm mass	H/C	Lower Heating Value MJ/kg	Fuel Density (20 C) kg/m^3
JP-8 4/25/13	85.83	13.62	344	1.89	43.2	809
JP-8 4/29/13	85.91	13.81	219	1.92	43.0	802
Camelina	85.31	14.42	81	2.01	43.3	778

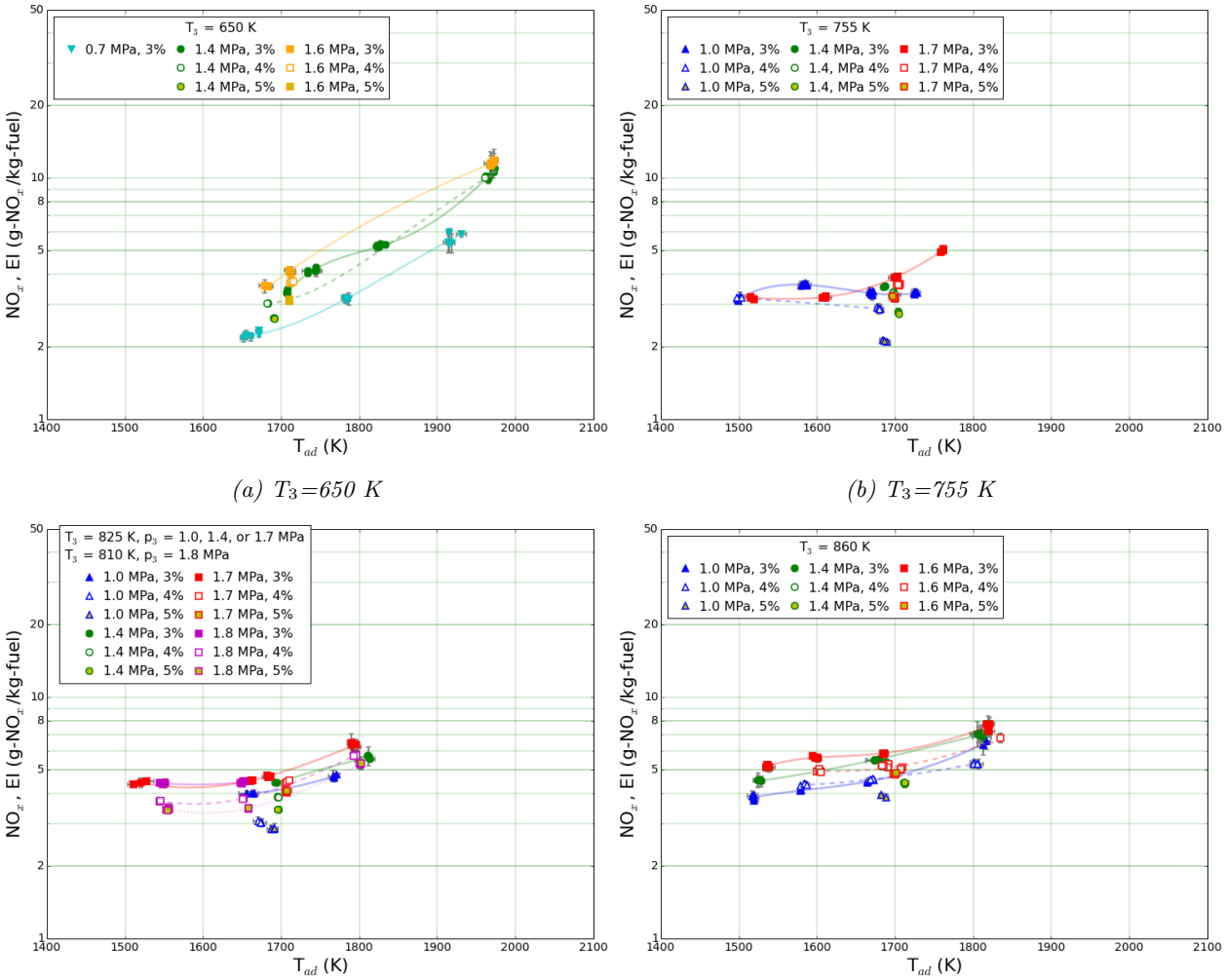

(a) T_3=650 K

(b) T_3=755 K

(c) T_3=810–825K

(d) T_3=860

Figure 8: *Flat dome configuration. NO_x emissions as a function of equilibrium flame temperature T_{ad} at constant T_3: (a) 650 K, (b) 755 K, and (c) 810–825 K, and (d) 860 K.*

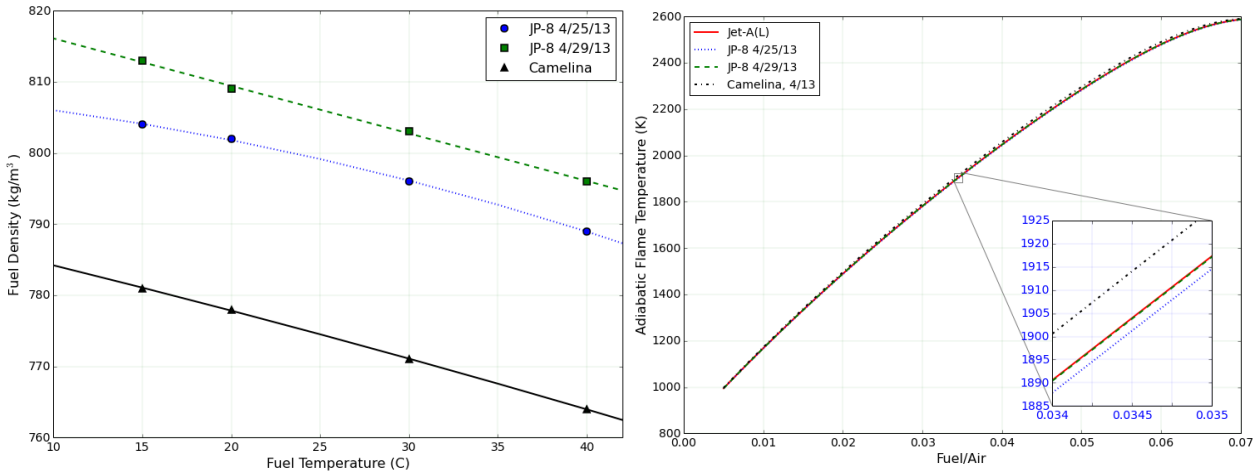

(a) Fuel density

(b) Adiabatic flame temperature

Figure 9: *Comparison of JP-8 and Camelina fuels.*

independent of alternative fuel concentration. In other words, using the Camelina biofuel in place of JP-8 does not affect NO_x emissions. Since the properties of JP-8 and Camelina are similar, this is not surprising.

E. NO_x Correlation Equations and ICAO NO_x Emissions

In this section, correlation equations are developed for the flat dome configuration. Correlation equations are used to estimate NO_x emissions at conditions that were not tested. Since the NASA flametube could not reach the inlet conditions needed for high power operation, the correlation equations are needed to estimate the landing-takeoff NO_x emissions.

Since the second generation SV-LDI hardware was based on the baseline SV-LDI hardware, the flat dome NO_x emissions are first compared to the emissions predicted by baseline correlation equations. Then, correlation equations are developed for the second generation flat dome configuration. Finally, the correlation equations are used to estimate the ICAO landing-takeoff NO_x emissions.

1. Comparison with the baseline correlation equations

Since the second generation SV-LDI configurations are based on the original baseline 9-point SV-LDI configuration, the second generation correlation equations will be based on the baseline correlation equations developed in R. Tacina et al.[1] The baseline correlations are given in equations 1–3 below, where T_3 is in Kelvin, p_3 is in kPa, and $\Delta p/p$ is in %:

$$\text{EI-NOx} = a_1\, p_3^{0.50} e^{T_3/230} \phi^{b_1} \left(\frac{\Delta p}{p}\right)^{-0.60} \tag{1}$$

$$\text{EI-NOx} = a_2\, p_3^{0.59} e^{T_3/194} \phi^{b_2} \left(\frac{\Delta p}{p}\right)^{-0.56} \tag{2}$$

$$\text{EI-NOx} = a_3\, p_3^{0.50} e^{T_3/230} e^{T_{ad}/b_3} \left(\frac{\Delta p}{p}\right)^{-0.60} \tag{3}$$

The correlation equations described by equations 1, 2, and 3 will be referred to as Fit 1, Fit 2, and Fit 3, respectively. The coefficients a and b are given in Table 4 for two baseline 9-point SV-LDI configurations: the configuration with a 60° swirler angle and co-rotating swirlers and the configuration with a 45° swirler angle and co-rotating swirlers. The coefficient of determination, R^2, for each correlation is also given. The correlation equations capture the trends in the baseline NO_x emissions quite well: the R^2 value for each correlation are above 0.9 (1.0 would indicate a "perfect fit") and Fig. 11 shows that the NO_x predicted by the correlation equations is close to the measured NO_x.

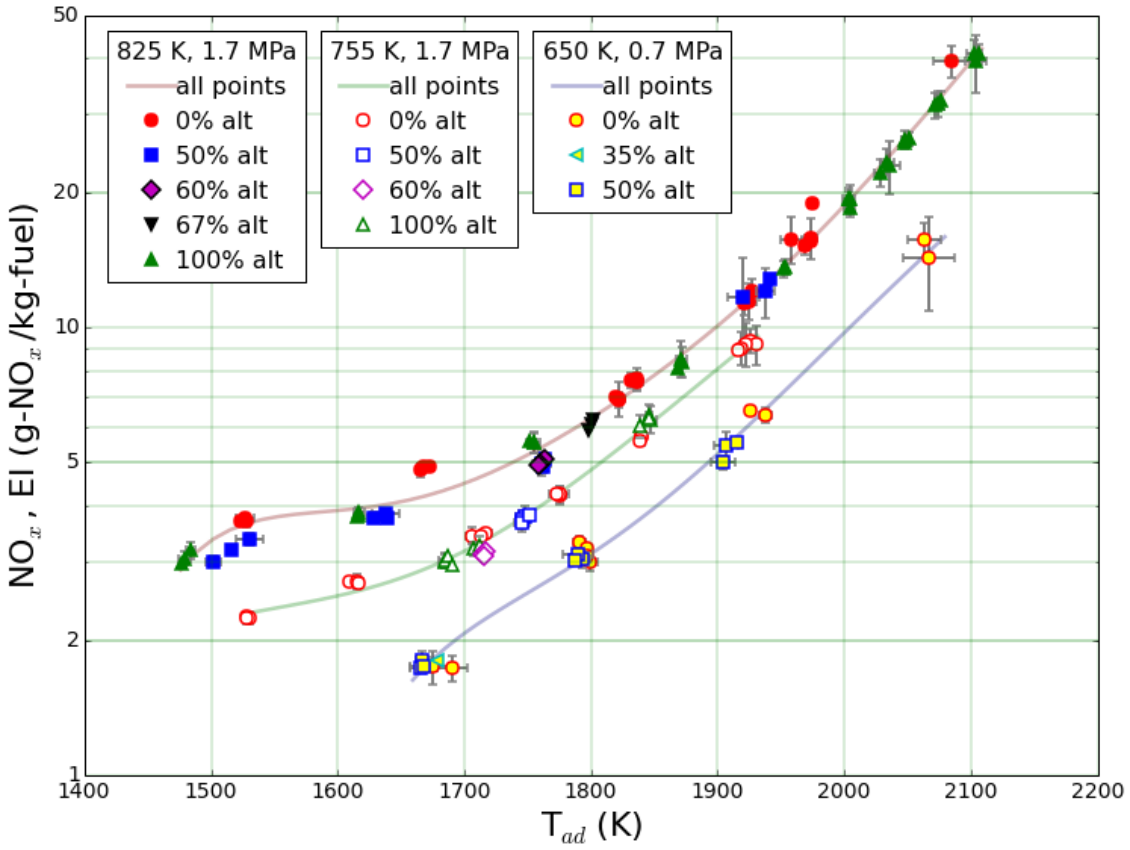

Figure 10: *Effect of alternative fuel. For all cases, $\Delta p/p$=3.2%*

Table 4: *Baseline and flat dome correlation equations.*

Configuration	Fit 1			Fit 2			Fit 3		
	a_1	b_1	R_1^2	a_2	b_2	R_2^2	a_3	b_3	R_3^2
Baseline, 60°	0.06	1.60	0.97	0.013	1.69	0.93	0.0014	520	0.98
Baseline, 45°	0.4	4.82	0.98	0.11	5.07	0.98	1.0×10^{-6}	178	0.95
Flat Dome	0.106	2.82	0.63	0.0378	3.20	0.55	5.52×10^{-5}	279	0.65

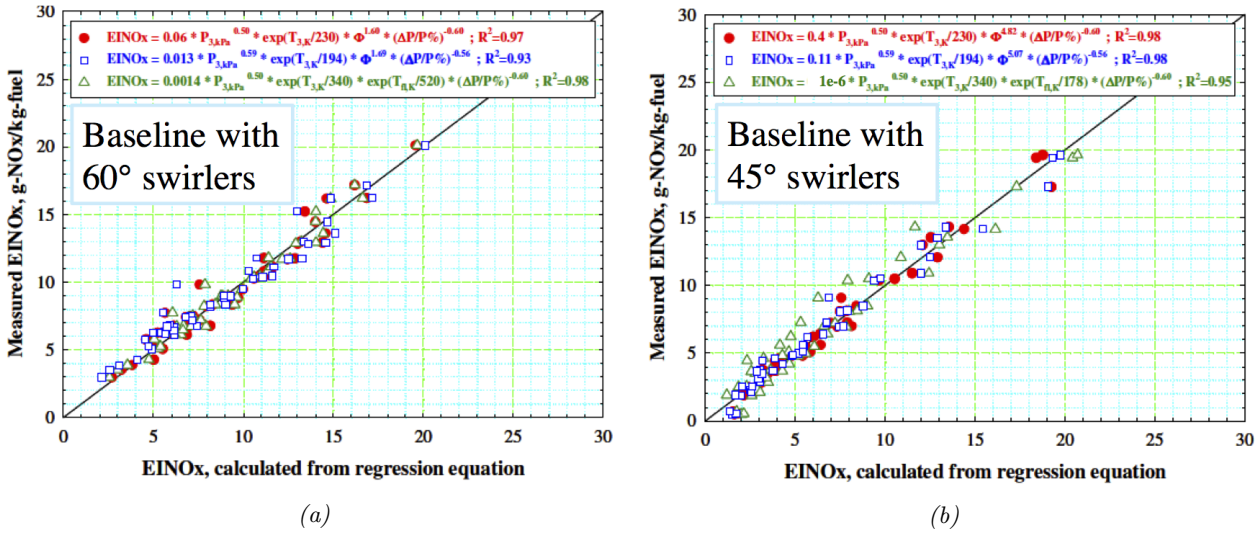

(a) *(b)*

Figure 11: *Correlation equations for the baseline 9-point SV-LDI design with (a) 60° co-rotating swirlers and (b) 45° co-rotating swirlers. From R. Tacina et al.*[1]

Before finding the coefficients a and b for the flat dome configuration, the NO_x emissions for the flat dome configuration were first compared to the predictions from the baseline correlation equations. This was done to check that the correlation equations give reasonable results for the flat dome configuration. The swirler angles for the flat dome configuration were all between 45° and 60°, so it is expected that the flat dome NO_x emissions will fall between the NO_x emissions predicted for the baseline configuration with 45° swirlers and that for 60° swirlers.

Before comparing the flat dome NO_x emissions to the baseline 45° and 60° curve fits, the baseline curve fits will be compared to each other. This will be done by taking the ratio of each curve fit for the 45° swirlers to the corresponding curve fit for the 60° swirlers. These ratios will be called r_1, r_2, and r_3. For example, r_1 is the ratio of Fit 1 for the 45° swirlers to Fit 1 for the 60° swirlers. Taking these ratios shows that the ratios of Fits 1 and 2, r_1 and r_2, are functions only of the equivalence ratio and that the ratio of the Fit 3s, r_3, is a function only of the equivalence ratio. This is shown in equations 4–6 below; in these equations the a and b values for each fit come from Table 4.

$$\text{Fit 1: } 45^\circ \text{ NO}_x/60^\circ \text{ NO}_x\text{: } r_1 = \frac{a_{1,45^\circ}\phi^{b_{1,45^\circ}}}{a_{1,60^\circ}\phi^{b_{1,60^\circ}}} = \frac{0.4\phi^{4.82}}{0.06\phi^{1.60}} \tag{4}$$

$$\text{Fit 2: } 45^\circ \text{ NO}_x/60^\circ \text{ NO}_x\text{: } r_2 = \frac{a_{2,45^\circ}\phi^{b_{2,45^\circ}}}{a_{2,60^\circ}\phi^{b_{2,60^\circ}}} = \frac{0.11\phi^{5.07}}{0.013\phi^{1.69}} \tag{5}$$

$$\text{Fit 3: } 45^\circ \text{ NO}_x/60^\circ \text{ NO}_x\text{: } r_3 = \frac{a_{3,45^\circ}e^{T_{ad}/b_{3,45^\circ}}}{a_{2,60^\circ}e^{T_{ad}/b_{3,60^\circ}}} = \frac{10^{-6}e^{T_{ad}/178}}{0.0014e^{T_{ad}/520}} \tag{6}$$

Calculating these ratios according to equations 4–6 indicates that the NO_x emissions from the 45° baseline configuration will be less than those from the 60° configuration at low equivalence ratios and flame temperatures. However, as the equivalence ratio and flame temperature increase, the 45° configuration will have higher NO_x emissions; this will occur at $\phi > \sim 0.55$ and $T_{ad} > \sim 1950$. This result is consistent with the measurements reported in R. Tacina et al.[1]

Since the swirler angles for the flat dome configuration were all between 45° and 60°, the flat dome configuration is expected to have higher NO_x emissions than the 45° baseline curve fits at low equivalence ratios but similar or lower NO_x emissions at higher equivalence ratios. Similarly, the flat dome configuration is expected to have lower NO_x emissions than the 60° baseline curve fits at low equivalence ratios but similar or higher NO_x emissions at higher equivalence ratios.

The results show that this is what happens. Figure 12 shows the measured flat dome NO_x emissions compared to the baseline correlation equations. The color of each symbols indicates the equivalence ratio ϕ at that point, with blue symbols at the lowest equivalence ratios and red symbols at the highest equivalence

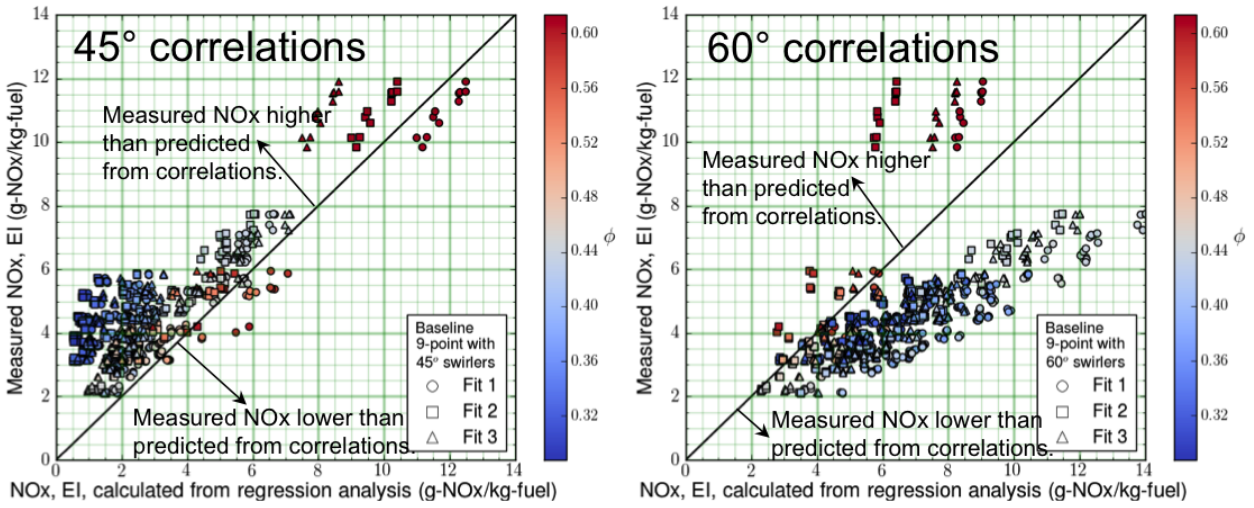

Figure 12: *Comparison of the measured NO_x emissions from the flat dome SV-LDI design to the emissions predicted by the baseline 9-point SV-LDI design with (a) 45° and (b) 60° swirlers.*

ratios. Figure 12a compares the flat dome NO_x emissions to the baseline 45° correlation equations. As expected, at low equivalence ratios (blue symbols), the flat dome NO_x emissions are higher than predicted by the correlation equation, but at high equivalence ratios (red symbols), the NO_x emissions are lower. Figure 12b compares the flat dome NO_x to the baseline 60° correlation equations. Again as expected, the flat dome NO_x emissions are lower than the predicted by the 60° correlations at low equivalence ratios, but about the same or slightly higher than predicted at high equivalence ratios.

These results show that baseline correlation equations give reasonable results when compared to the measured flat dome NO_x emissions. Therefore, Fits 1–3 will be used as a basis for developing the flat dome correlation equations. This is done in the next section.

2. Flat dome correlation equations

Since the baseline correlation equations produced reasonable results when compared to the flat dome NO_x emissions data, these correlation equations were used as a basis for developing correlation equations for the flat dome configuration. First, multiple regression was used to find the coefficients a and b for Fits 1–3. This regression was done only on points where the fuel-air ratio was the same for each stage. The coefficients a and b for each of Fits 1–3 are given in Table 4. However, results show that Fits 1–3 do not adequately describe the NO_x emissions data: the R^2 values were all below 0.7. The poor quality of the correlation from Fits 1–3 can also be seen in the plots in Fig. 13a.

In Fits 1–3, the effect of p_3, T_3, and $\Delta p/p$ were fixed at the values used for the baseline correlation equations. To see if the correlation equations would better describe the data if the effects of these variables were changed, two new correlation equations were developed, called Fits 4 and 5. For these equations, the exponents of p_3 and $\Delta p/p$ and the divisor of T_3 were allowed to vary. Multiple regression on data points with equal fuel staging was again done. The results are given in the equations for Fits 4 and 5 below:

$$\text{Fit 4: EI-NOx} = 0.255 p_3^{0.462} e^{T_3/314} \phi^{2.31} \left(\frac{\Delta p}{p}\right)^{-0.695}, \qquad R^2 = 0.67 \tag{7}$$

$$\text{Fit 5: EI-NOx} = 0.0008 p_3^{0.460} e^{T_3/757} e^{T_{ad}/355} \left(\frac{\Delta p}{p}\right)^{-0.647}, \qquad R^2 = 0.77 \tag{8}$$

Although Fits 4 and 5 described the data slightly better – R^2 was a bit higher – they still did not describe the data well. R^2 was below 0.8 for both Fit 4 and 5, and plots of the measured NO_x vs. the NO_x calculated from Fits 4 and 5 show that these fits did not collapse the data. See Fig. 13b.

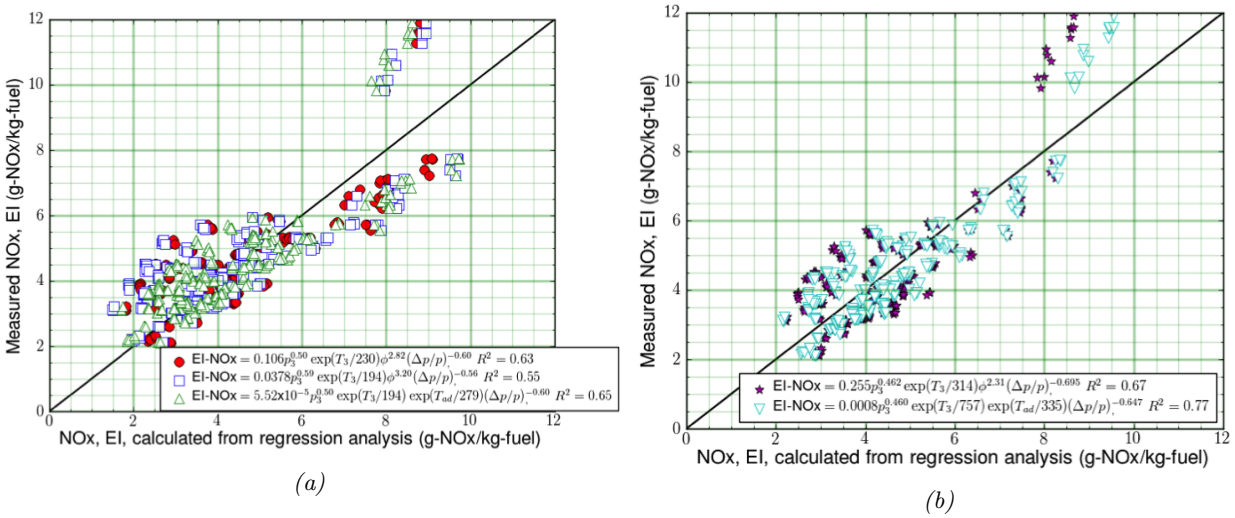

Figure 13: *Correlation equations for the flat dome SV-LDI design.*

An explanation for why Fits 1–5 do not adequately describe the flat dome NO_x emissions can be found by comparing the flat dome SV-LDI geometry to the baseline 9-point geometry. For the baseline 9-point configuration, all fuel/air mixers were identical in fuel injector type, swirler angle, and venturi geometry. However, the fuel/air mixers for the flat dome configuration were not identical: they differed in fuel injector type, swirler angle, and venturi geometry. These differences in fuel/air mixer could result in each type of fuel/air mixer following a different correlation; the CFD results of Ajmani et al[15] show that this is indeed the case. Therefore, Fits 1–4 were modified to have a term for each stage in which the fuel-air ratio could be varied independently. Since the fuel lines for main stages 2 and 3 were ganged together, this results in a term for the pilot, a term for main 1, and a term for mains 2 and 3. The total NO_x emissions are found by adding the three terms together. In other words,

$$\mathrm{NO_x} = (\mathrm{NO_x})_{\mathrm{pilot}} + (\mathrm{NO_x})_{\mathrm{main\ 1}} + (\mathrm{NO_x})_{\mathrm{mains\ 2\ \&\ 3}} \tag{9}$$

This results in the modified correlation equations Fits 1n–5n, as given below:

$$\text{Fit 1n: EI-NOx} = p_3^{0.50}\, e^{T_3/230} \left(\frac{\Delta p}{p}\right)^{-0.60} \sum_{i=1}^{3} a_{1n,i}\phi_{1n,i}^{b} \tag{10}$$

$$\text{Fit 2n: EI-NOx} = p_3^{0.59}\, e^{T_3/194} \left(\frac{\Delta p}{p}\right)^{-0.56} \sum_{i=1}^{3} a_{2n,i}\phi_{2n,i}^{b} \tag{11}$$

$$\text{Fit 3n: EI-NOx} = p_3^{0.50}\, e^{T_3/340} \left(\frac{\Delta p}{p}\right)^{-0.60} \sum_{i=1}^{3} a_{3n,i}e^{T_{\mathrm{ad}}b_{3n,i}} \tag{12}$$

$$\text{Fit 4n: EI-NOx} = p_3^{0.46}\, e^{T_3/314} \left(\frac{\Delta p}{p}\right)^{-0.695} \sum_{i=1}^{3} a_{4n,i}\phi_{4n,i}^{b} \tag{13}$$

$$\text{Fit 5n: EI-NOx} = p_3^{0.46}\, e^{T_3/757} \left(\frac{\Delta p}{p}\right)^{-0.647} \sum_{i=1}^{3} a_{5n,i}e^{T_{\mathrm{ad}}b_{5n,i}} \tag{14}$$

where $i = 1$ indicates the pilot stage, $i = 2$ indicates the main 1 stage, and $i = 3$ indicates the main 2 and 3 stages.

Multiple regression was again done, this time including results where the fuel-air ratio was not the same for each stage. Fits 1n–5n capture the data much better, with R^2 values typically above 0.9. Examining the plots of measured vs. calculated NO_x emissions showed that Fits 1n and 2n appear to capture the data best; this is shown in Fig. 14. The coefficients $a_{1n,i}$ and $a_{2n,i}$ and the R^2 value for Fits 1n and 2n are shown

Table 5: *Coefficients for Fits 1n and 2n*

Correlation Equation	$a_{f,1}$	$b_{f,1}$	$a_{f,2}$	$b_{f,2}$	$a_{f,3}$	$b_{f,3}$	R^2
Fit 1n, f =1n	0.0081	0.29	0.350	7.15	0.369	7.37	0.950
Fit 2n, f =2n	0.0024	0.453	0.0958	7.56	0.190	8.04	0.926

in Table 5. Since these two fits capture the data well, they will be used to calculate the landing-takeoff NO_x emissions.

3. Landing-takeoff NO_x emissions

The landing-takeoff NO_x emissions were calculated for the flat dome configuration. The Pratt & Whitney ERA cycle conditions were used, and we assumed 20% liner cooling. For the lower power conditions, the flametube measurements were used to find the NO_x emissions. For the higher power points, correlation equations Fit 1n and Fit 2n were used. The flat dome NO_x emissions were 87–88% below the CAEP/6 standards. This exceeds the ERA project goal of 75% NO_x reduction.

IV. Future Work

There are five areas where future work will be done. 1) The third second generation LDI configuration developed by Woodward will be tested in NASA's flametube test rig. 2) A active combustion control scheme developed by Woodward will be tested in the NASA flametube. 3) Measurements when the fuel-air ratios were different for each stage will be further analyzed and reported. 4) The measurements taken at near-idle conditions will be reported. 5) The dynamic pressure measurements will be further analyzed and reported.

V. Summary

Three second generation SV-LDI configurations were developed. All were based on the baseline 9-point SV-LDI configuration reported previously.[1] These second generation configurations had better low power operability than the baseline 9-point configuration. Two of these second generation configurations were tested in a NASA Glenn Research Center flametube; these two configurations are called the flat dome and 5-recess configurations. Results show that the 5-recess configuration generally had lower NO_x emissions than the flat dome configuration. Correlation equations were developed for the flat dome configuration so that the landing-takeoff NO_x emissions could be estimated. The flat dome landing-takeoff NO_x is estimated to be 87–88% below the CAEP/6 standards, exceeding the ERA project goal of 75% reduction.

Acknowledgments

Thanks to the engineering and technician staff for NASA's CE-5 test rig: Derek Podboy, Tom Barkis, Bill Rozman, Harold Redloske, and Daniel Washington.

This project was funded by NASA's Environmentally Responsible Aviation (ERA) project in the Integrated Systems Research Program (ISRP).

References

[1]Tacina, R., Lee, P., and Wey, C., "A Lean-Direct-Injection Combustor Using a 9 Point Swirl-Venturi Fuel Injector," ISABE-2005-1106, 2005.

[2]Lee, D., Pitari, G., Grewe, V., Grierens, K., Penner, J., Petzold, A., Prather, M., Schumann, U., Bais, A., Berntsen, T., Iachetti, D., Lim, L., and Sausen, R., "Transport impacts on atmosphere and climate: Aviation," *Atmospheric Environment*, Vol. 44, 2010, pp. 4678–4734.

[3]Tacina, R. R., "Low-NOx Potential of Gas Turbine Engines," AIAA-1989-0550, 1989.

[4]Chang, C. and Holdeman, J., "Low Emissions RQL Flametube Combustor Test Results," NASA/TM–2001-211107., 2001.

[5]Peterson, C., Sowa, W., and Samuelson, G., "Performance of a Model Rich Burn–Quick Mix–Lean Burn Combustor at Elevated Temperature and Pressure," NASA/CR–2002-21192, 2002.

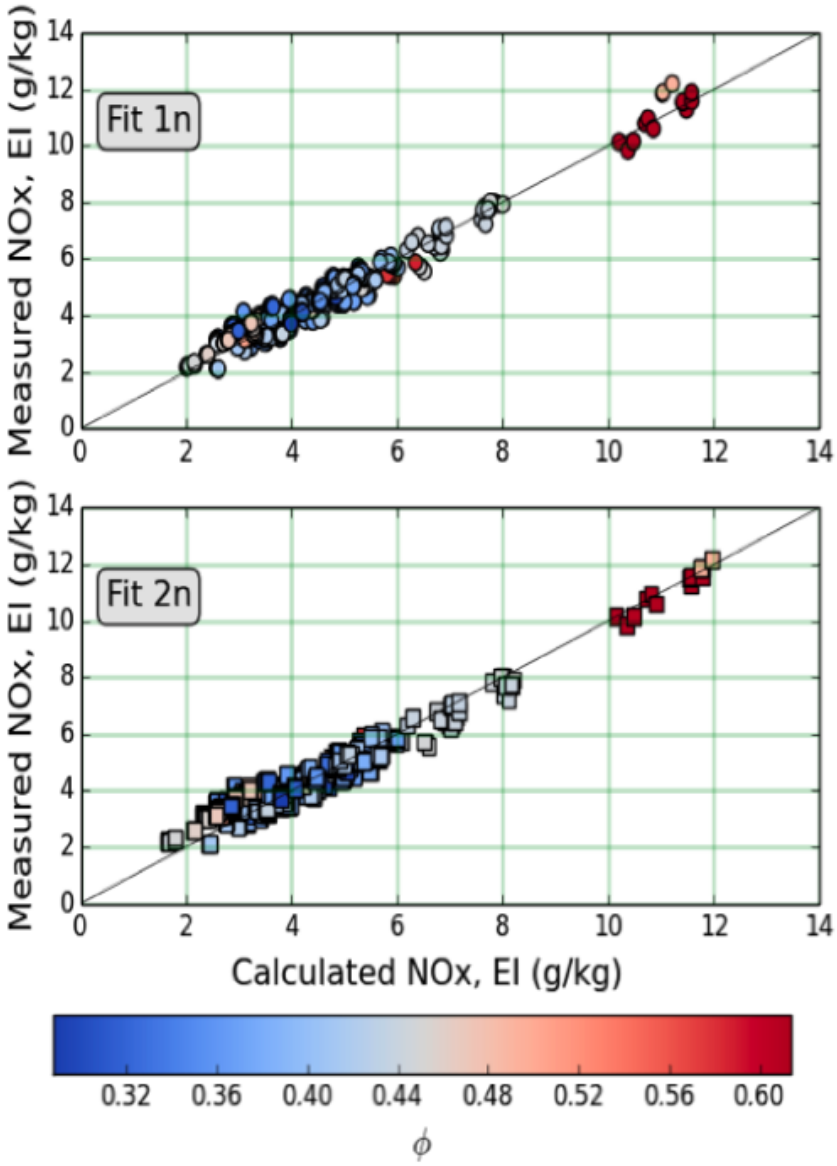

Figure 14: *Correlation equations for the flat dome SV-LDI design.*

[6]Lee, C.-M., Bianco, J., Deur, J., and Ghorashi, B., "Nitric Oxide Formation in a Lean Premixed Prevaporized Jet A/Air Flame Tube: an Experimental and Analytical Study," NASA/TM–2001-105722, 1992.

[7]Tacina, K. M., "Swirl-Venturi Lean Direct Injection Combustion Technology," Spring Technical Meeting of the Central States Section of the Combustion Institute, April 22–24, 2012.

[8]Tacina, R., Wey, C., Laing, P., and Mansour, A., "A Low-NOx Lean-Direct Injection, MultiPoint Integrated Module Combustor Concept for Advanced Aircraft Gas Turbines," NASA/TM–2002-211347, 2005.

[9]Tacina, R., Mao, C.-P., and Wey, C., "Experimental Investigation of a Multiplex Fuel Injector Module with Discrete Jet Swirlers for Low Emissions Combustors," AIAA-2004-0135, 2004.

[10]Hicks, Y. R., Heath, C. M., Anderson, R. C., and Tacina, K. M., "Investigations of a combustor using a 9-point swirl-venturi fuel injector: recent experimental results." ISABE-2011-1106, 2011.

[11] "Procedure for the Continuous Sampling and Measurement of Gaseous Emissions from Aircraft Turbine Engines," SAE/ARP1256D 2011-07, 2011.

[12]Bianco, J., "NASA Lewis Research Center's Combustor Test Facilities and Capabilities," AIAA -1995-2681, 1995.

[13] "Procedure for the Analysis and Evaluation of Gaseous Emissions from Aircraft Engines," SAE/ARP1533B 2013-01, 2013.

[14]Gordon, S. and McBride, B. J., "Computer Program for Calculation of Complex Chemical Equilibrium Compositions and Applications I. Analysis," NASA RP-1311, 1994.

[15]Ajmani, K., Mongia, H., and Lee, P., "CFD Computations of Emissions for LDI-2 Combustors with Simplex and Airblast Injectors," AIAA-2014-3529, 2014.